Hindawi
Journal of Nanomaterials
Volume 2020, Article ID 6189061, 10 pages
https://doi.org/10.1155/2020/6189061

Research Article

Urea-Assisted Synthesis of Nanospherical and Plate-Like Magnesium Oxides for Efficient Removal of Reactive Dye Wastes

H. M. S. P. Randiligama,[1] **M. M. M. G. P. G. Mantilaka**,[1,2] **and T. C. Palihawadana**[2]

[1]*Postgraduate Institute of Science, University of Peradeniya, University of Peradeniya, Kandy 20400, Sri Lanka*
[2]*Sri Lanka Institute of Nanotechnology, Nanotechnology and Science Park, Mahenwatte, Pitipana, Homagama, Sri Lanka*

Correspondence should be addressed to M. M. M. G. P. G. Mantilaka; mantilaka@gmail.com

Received 27 May 2020; Revised 28 October 2020; Accepted 23 November 2020; Published 17 December 2020

Academic Editor: Tetiana Dontsova

Nanospherical and plate-like magnesium oxide has been successfully synthesized by urea precipitation method for the first time. A magnesium oxide precursor was prepared by heating MgCl2 solution with urea for 12 hours at 90°C. Then the calcined precursor was analysed by Scanning electron microscopy (SEM), X-ray diffraction (XRD), Fourier transform infrared (FT-IR) spectroscopy, thermogravimetric analysis (TGA), and high-resolution transmission electron microscopy (HR-TEM). In the presence of the nonionic surfactant Triton X-100 in the system, the reaction yielded in nanospheres of MgO contrast to the plate-like MgO in the absence of the surfactant. The precursor and the calcined product appeared in similar morphologies under SEM in both cases with a slight reduction of size upon calcination. The final product was confirmed as MgO using XRD and FT-IR spectroscopic methods. In TGA, both samples showed similar mass loss values upon elimination of adsorbed water molecules and decomposition of the precursor into MgO; however, the nanospherical MgO sample showed an additional weight loss due to elimination of the associated surfactant molecules. The efficiency of removing reactive dye wastes was quantified by UV-visible spectroscopy using reactive yellow dye. Plate-like MgO showed a porous structure under HR-TEM analysis in the dye adsorption study, and both plate-like and nanospherical MgO showed good dye adsorption capability. MgO nanospheres showed higher capacity of dye adsorption compared to plate-like MgO, explained by its higher surface are-to-volume ratio, while the plate-like MgO also performed well due to having a nanoporous structure. These nanomaterials will offer high potential in purifying waste water and as well in recovering expensive dye products.

1. Introduction

Access to potable water is becoming a luxury due to exploitation of the limited amount of freshwater in Earth's freshwater reserves [1, 2]. Among all the major contributors to water pollution, industrial wastewater serves a major role towards the crisis by adding complex organic molecules which has the potential to be toxic to all ecosystems, including human [1–3]. With the growing demand for the fashionable and advanced textile products around the globe, it has become an inevitable fact that various forms of industrial dyes are being used in apparels industry. Until 1850, all important colours were obtained by natural dyes and after Perkin's invention synthetic dye substituted their role. Present statistics related to colour index states that there are approximately 10000 types of being manufactured with more than 700000 tons of annual production [4]. Reactive dyes are one of the most widespread dyes used in colouring textiles because they offer greater stability and durability in contrast to other dyes by making covalent bonds between dye molecules and the cellulose or protein fibers [5–8].

Escalating consumer demands followed by rapid industrial growth versus the global water crisis lead to a real-world conundrum which leads research on water purification to be timely and urgent. Thus, a solution from a biocompatible, nontoxic, inexpensive, and readily available product becomes a worth focus. In the last few years, numerous removal methods have been introduced: physical methods such as adsorption, coagulation-flocculation, and membrane filtration and chemical methods such as ion exchange,

chemical precipitation, oxidation, and catalytic degradation as well as chemical methods such as biological degradation account for treatment methods [9, 10]. Due to high stability towards light, heat and oxidizing agent dyes are resistant to degradation [11]. Among these methods, adsorption is considered the most efficient due to its simplicity and economical ease.

Magnesium oxide (MgO) or magnesia is an inorganic metal oxide material, available in its natural form as periclase as well as a synthetic chemical product. Natural MgO, periclase, is mainly used as a refractory material due to its high thermal and chemical stability even at very high temperatures [9, 10]. Magnesium is found in seawater as MgCl2, as the second most abundant chloride, next to sodium chloride [12]. Large quantities of magnesium chloride are extracted from seawater, where it serves as the starting material for many of the magnesium compounds. Magnesium oxide nanoparticles (MgO-Nps) are synthesized by various methods such as sol gel method [13–15], sonochemical methods [16], microwave methods [17, 18], biosynthetic methods [19], laser ablation [20], and precursor methods [20–22]. MgO-Nps are used in a broad range of applications such as for carbon monoxide and sulfur dioxide adsorption [23–25], dye adsorption and degradation [5, 26–29], heavy metal removal [30], and photocatalysis [31, 32].

This study focuses on a novel and facile approach which is also easily upscalable to produce larger quantities of spherical magnesium dioxide nanoparticles of narrow particle size distribution and plate-like magnesium dioxide with fine nanoporous structure, using the readily available magnesium chloride as the magnesium source. The simplicity and the upscalability of this process, use of a readily available magnesium compound as the magnesium source, and use of inexpensive and nontoxic chemicals for the synthesis of nanospherical and plate-like nanoporous magnesium oxide morphologies with the high-quality controllability make this novel approach a distinct process with a higher commercial viability. Further, reduction efficiency for commercially available Remazol yellow 3RS by synthesized MgO-Nps is studied.

2. Materials and Methods

2.1. Materials. Urea (99% purity), anhydrous magnesium chloride (99.5% purity), and Triton X-100 (99% purity) surfactant were purchased from Sigma-Aldrich. Remazol yellow 3RS (reactive yellow) (Figure 1) textile dye was kindly donated by Textured Jersey Pvt. Ltd., Sri Lanka. The dye was used without further purification.

2.2. Synthesis of Plate-Like MgO. 100 mL of 1 M urea solution was added into 100 mL of 1 M $MgCl_2$ solution in a round bottomed flask equipped with refluxing condenser while stirring. The mixture was heated at 90°C for 12 h with continuous stirring. The precipitated precursor was washed with 50 mL of distilled water for 3 times and was dried at 120°C for 2 h. The precursor particles were then calcined at 520°C for 3 h to produce MgO particles.

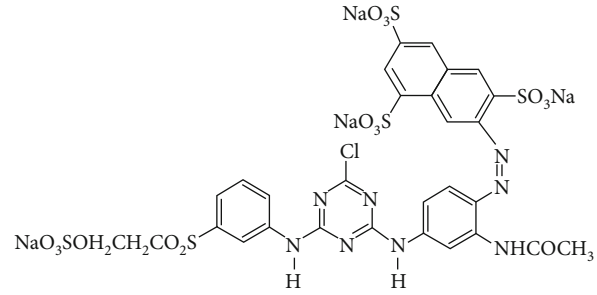

Figure 1: Remazol yellow 3RS (reactive yellow) dye molecule.

2.3. Synthesis of Nanospherical MgO. 100 mL of 1 M urea solution was added into 100 mL of 1 M $MgCl_2$ solution in a round bottomed flask equipped with refluxing condenser while stirring. 0.2 mL of Triton X-100 was added to the mixture and stirred until the formation of Triton X-100 micelles. The mixture was heated at 90°C for 12 h to obtain precipitated precursor particles. The precursor particles were separated out by centrifuging, washed with distilled water for 3 times, and dried in an oven at 120°C for 2 h. The dried precursor particles were calcined at 520°C for 3 h to synthesize MgO nanoparticles.

2.4. Characterization of Synthesized Materials

2.4.1. Morphological Analysis. The morphologies of precursors, synthesized MgO, and RY-adsorbed MgO samples were observed with the aid of Hitachi SU6600 field-emission scanning electron microscope (FE-SEM) with an acceleration voltage of 15 kV. Samples were well coated with a gold thin-film before the analysis.

2.4.2. X-Ray Diffraction Studies. Crystalline phases of products and precursors were characterized using X-ray diffraction (XRD) with the aid of Bruker, Focus D8 X-ray diffractometer (CuKα radiation wavelength, $\lambda = 0.1540562$ nm and scanning rate of 1 mn^{-1}). The average crystallite size of MgO products was calculated using the Debye-Scherrer equation to the major XRD peak of MgO, as given in Equation (1).

$$D = \frac{0.89\lambda}{\beta \cos \theta}, \quad (1)$$

where λ is the X-ray wavelength of the CuKα radiation ($\lambda = 1.54$ Å), β is the full width at half maximum of the XRD major peak, and θ is the angle of diffraction.

2.4.3. Fourier Transform Infrared Spectroscopy. Fourier transform infrared (FT-IR) spectroscopy was used to study adsorption and bonding nature of RY on synthesized MgO samples. The FT-IR spectra of samples were recorded on the Bruker Vertex 80 instrument within wavenumber range 500–4000 cm^{-1} with 32 scans per measurement at 0.4 cm^{-1} resolution.

2.4.4. Thermal Characteristics of Precursors. Thermal decomposition of precursors was analysed using thermogravimetric

analysis (TGA) (STD Q600). The samples were heated from 25 to 800°C at a heating rate of 15°C/min in nitrogen environment.

2.4.5. Analysis of Porosity of MgO Products. Pores of plate-like MgO particles was observed using the Jeol 2100 high-resolution transmission electron microscope (HR-TEM).

2.4.6. Dye Adsorption Studies. RY dye solutions of different concentrations (100, 200, 400, 600, 800, and 1000 ppm) were prepared by dissolving RY in deionized water. 0.005 g of synthesized MgO particles was added into 10 mL of each dye solution. The mixture was well shaken and kept for equilibrium for 30 min. The precipitated dye-adsorbed MgO particles were separated out from the solution by decantation. The final dye concentrations of supernatants were analysed using UV-vis spectrophotometer (Shimadzu UV-3600) at λ max of the RY at 416 nm. The equilibrium dye adsorption capacity (Q_e) of the prepared MgO samples was calculated with the Equation (2).

$$Q_e = \frac{(C_0 - C_e)}{m}, \tag{2}$$

where, C_0 is the initial concentration, C_e is equilibrium concentration after adsorption of RY, V is volume of the dye solution, and m is the mass of the MgO adsorbent.

Interactions between adsorbate molecules and adsorbent surface were studied using most widely used the Langmuir isotherm and Freundlich isotherm. The Langmuir adsorption isotherm can be expressed as that in Equation (3).

$$\frac{C_e}{Q_e} = \frac{1}{K_L Q_m} + \frac{1}{Q_m} C_e, \tag{3}$$

where Q_m is the theoretical maximum monolayer sorption capacity and K_L is a coefficient on energy of sorption. Q_m and K_L were calculated by drawing a plot between C_e/Q_e and C_e. The Langmuir adsorption isotherm assumes that adsorption occurs at specific homogeneous sites of the adsorbent, and once the dye molecule occupies a site, there is no additional adsorption that could take place there which means monolayer sorption is assumed in the Langmuir isotherm. Multilayer adsorption is predicted by the Freundlich adsorption isotherm which is expressed as that in Equation (4).

$$lnQ_e = lnK_F + \frac{1}{n} lnC_e, \tag{4}$$

where n is a heterogeneous factor and K_F is a constant showing degree of adsorption. These constants were calculated by drawing a graph between ln Q_e vs. ln C_e.

Desorption study was carried out by dispersing 0.01 g of each RY-adsorbed MgO product into 10 mL of doubly distilled water followed by shaking. The supernatant was collected and analysed using the UV-vis spectrometer. RY-adsorbed MgO particles were characterized using FT-IR, XRD, and SEM to understand the adsorption mechanism.

3. Results and Discussion

3.1. Characterization of Precursors and MgO Products. SEM images as depicted in Figures 2(a) and 2(b) show that the precursor and MgO product prepared in the absence of Triton X-100 surfactant are in plate-like morphology, respectively. The precursor and MgO particles prepared in the presence of the surfactant are of spherical morphology as observed in Figures 2(c) and 2(d), respectively. The particle size distribution of spherical precursor and spherical MgO is shown in Figures 2(e) and 2(f), respectively. The highest particle size distribution of spherical precursor is obtained in the range of 41-60 nm. The highest particle size distribution of spherical MgO nanoparticles is in the range of 61-80 nm. The particle size of spherical MgO has been increased due to the particle aggregation at the calcination stage. However, spherical MgO nanoparticles are distributed in narrow size range compared to their precursor particles. Moreover, the transmission electron microscopic images in Figures 2(g) and 2(h) depict the nanopores of 5-10 nm range in plate-like MgO created during the calcination stage of the precursor.

XRD patterns of precursors and MgO materials are shown in Figure 3. Similar XRD patterns have been obtained for both precursors. These patterns are composed of peaks at 2θ values of 13.78°, 15.34°, 19.85°, 21.05°, 23.33°, 25.50°, 26.95°, 30.74°, 33.3.3°, 35.82°, 38.30°, 39.08°, 41.05°, 41.98°, 45.51°, 47.12°, 52.61°, and 56.71°.These peaks are matched with the standard XRD pattern of hydromagnesite [$Mg_4(OH)_2(CO_3)_3.3H_2O$] crystalline form with hexagonal lattice structure (JCPDS no. 08-0179).

During the synthesis procedure, urea has been hydrolysed into ammonium hydroxide and carbonate ions. These hydroxyl and carbonate ions have been reacted with Mg^{2+} ions in the reaction medium to form hydromagnesite precursors. According to the Debye-Scherrer formula which is applied to the major XRD peak of precursor particles at (111) plane, crystallite sizes of precursor in the absence and presence of Triton X-100 are 43 nm and 27 nm, respectively. XRD patterns of final products obtained after calcination of precursors at 520°C are composed of peaks at 2θ values of 36.78°, 42.73°, and 62.17°. These peaks can be assigned to the standard XRD pattern of the periclase crystalline form of MgO with cubic lattice structure (JCPDS Card No. 75-1525). As calculated using the Debye-Scherrer formula which is applied to the major XRD peak at (200) plane, crystallite sizes of MgO products obtained from precursors in the presence and in the absence of Triton 4X-100 are 27 nm and 23 nm, respectively.

Figure 4 shows the FT-IR spectra of synthesized MgO products. FT-IR spectra further confirm the presence of MgO in the final products. The high intensity major IR absorption band of both spectra at 545 cm^{-1} corresponds to the Mg–O stretching vibration. The absorption band located at 3680 cm^{-1} and low-intensity band at 1610 cm^{-1} correspond to the O–H stretching and bending vibrations, respectively. These bands occur due to the surface-adsorbed water molecules of MgO particles. Another intensity band at 1037 cm^{-1} is found in FT-IR spectra which could be assigned to H^- ions on the surface of MgO particles. Surface-adsorbed $CO3^{2-}$

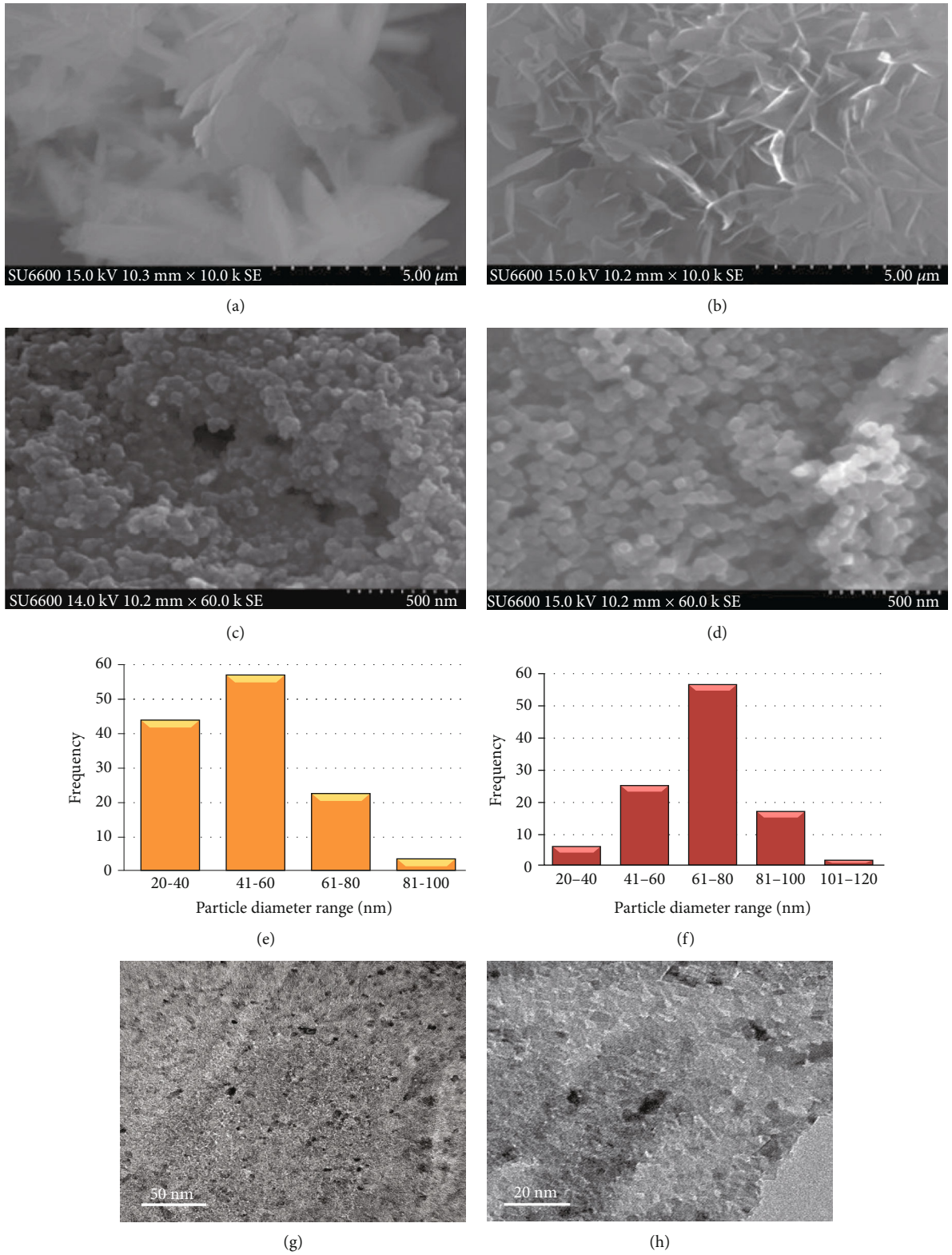

Figure 2: SEM images of (a) precursor in the absence of Triton X-100, (b) MgO prepared in the absence of Triton X-100, (c) precursor in the presence of Triton X-100, and (d) MgO prepared in the presence of Triton X-100, and particle size distribution of (e) precursor in the presence of Triton X-100 and (f) MgO nanospheres and (g), (h) TEM images of plate-like MgO.

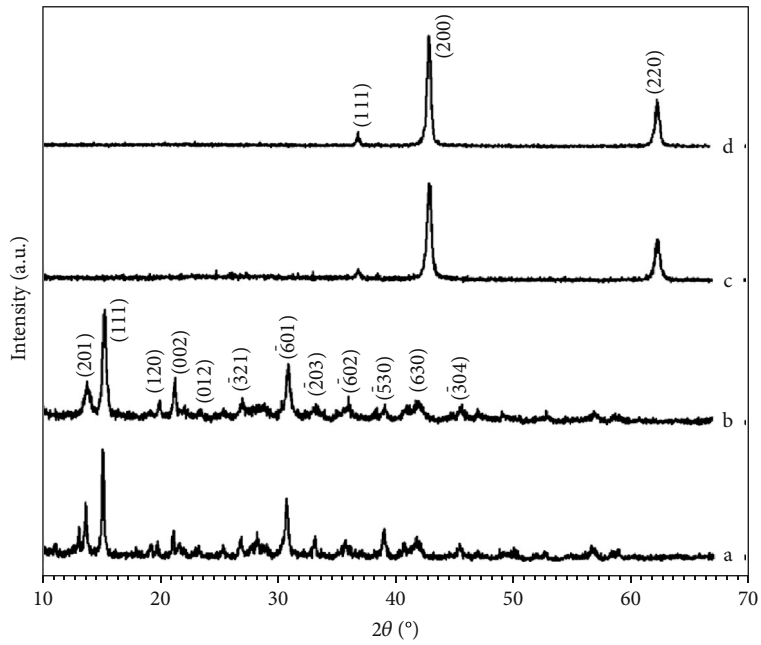

Figure 3: XRD pattern of (a) precursor in the absence of Triton X-100, (b) precursor in the presence of Triton X-100, (c) MgO prepared in the absence of Triton X-100, and (d) MgO.

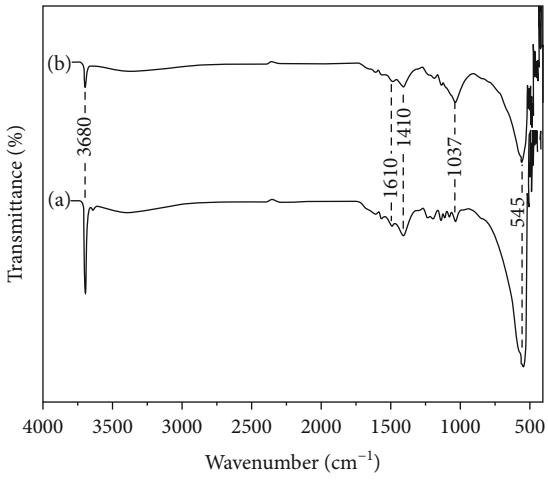

Figure 4: FT-IR spectra of (a) spherical MgO nanoparticles and (b) plate-like MgO.

ions of MgO particles are identified using the band at 1410 cm^{-1}. However, both water molecules and carbonate ions are found to be very low amounts as these bands have low intensity.

TGA plots of precursor particles are shown in Figure 5. The precursor particles of spherical MgO nanoparticles show a weight loss of 26% at the temperature 110°C which is due to the elimination of adsorbed water molecules. The weight loss of 16% at the temperature that ranges 215-272°C could be occurred due to the thermal degradation of associated surfactant molecules. The weight loss is 34% for spherical precursors at the temperature range 372-398°C. This weight loss is attributed to the thermal decomposition of Mg4(OH)2(-CO3)3.3H2O into MgO, CO2, and H2O. Similar sort of weight loss values are observed excluding the weight loss due to the degradation of surfactant in precursor of plate-like MgO with slightly different temperature ranges. These weight loss values of 6% and 36% have been obtained at temperatures of 224°C and 363-398°C, respectively. The elimination of CO2 and H2O from the precursor plates has led to nanopores which has made MgO products a great adsorption capacity.

3.2. Reactive Yellow Dye Adsorption Studies. UV-vis spectra of remaining RY dye concentrates after being adsorption by MgO products are given in Figures 6 and 7. Adsorption percentages of RY concentrations of 100, 200, 400, 600, 800, and 1000 ppm onto 0.005 g of nanospherical MgO are 100%, 95%, 77%, 64%, 57%, and 52%, respectively. At the same time, adsorption percentages of RY concentrations of 100, 200, 400, 600, 800, and 1000 ppm onto 0.005 g of plate-like MgO are 98%, 70%, 78%, 70%, 66%, and 53%, respectively. The photograph of the initial 400 ppm dye solution and the solution after the adsorption by nanospherical MgO is shown in Figure S1. Required plots for the evaluation of the adsorption isotherms are given in Figure S2 and Figure S3. Particular parameters of adsorption isotherms are given in Table 1.

Adsorption data are fitted to both the Langmuir and Freundlich isotherm models. However, the adsorption of RY in both MgO morphologies is a better fit to the Freundlich isotherm since the correlation coefficient (R^2) of the Freundlich isotherm is greater than that of the Langmuir isotherm. That means the adsorption of RY on to MgO particles follows a multilayer adsorption. The maximum adsorption capacity (Q_m) is found to be for plate-like MgO. However, there is no significant difference between values of maximum

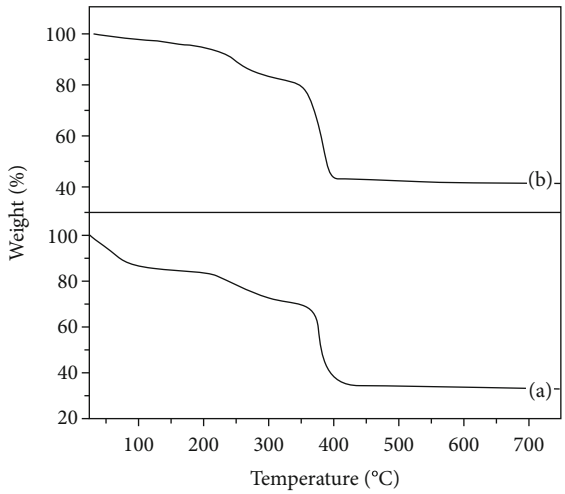

Figure 5: TGA plots of (a) spherical MgO nanoparticles and (b) plate-like MgO.

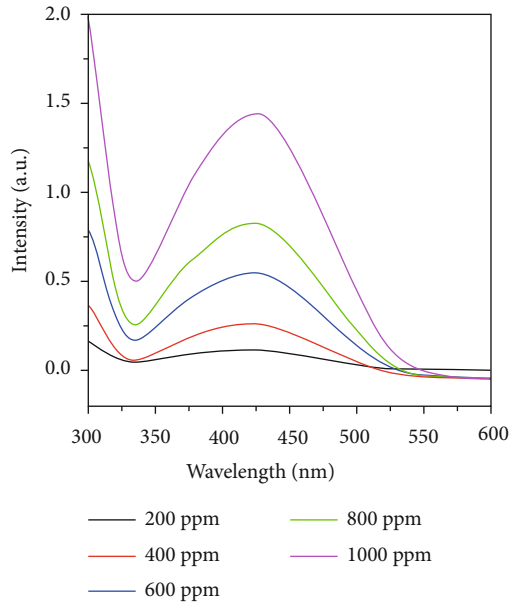

Figure 6: UV-vis spectra of various RY dye concentrations after being adsorbed by plate-like MgO.

adsorption capacities of nanospherical and plate-like MgO adsorbents. This data confirms that the adsorption performance of both morphologies is similar, and the key factor on adsorption performance of MgO is porosity and pore sizes.

3.3. Adsorption Kinetics. The kinetics of RY adsorption onto both nanospherical and plate-like MgO are fitted to the first-order kinetics as given by following Equation (5).

$$\ln\left(\frac{Q_e}{Q_t}\right) = kt, \tag{5}$$

where t is time and k is the rate constant.

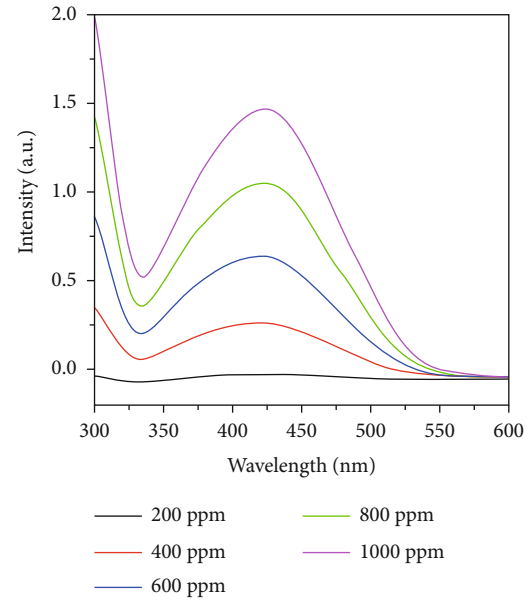

Figure 7: UV-vis spectra of various RY dye concentrations after being adsorbed by nanospherical MgO.

Table 1: Adsorption isotherms.

MgO material	Langmuir isotherm			Freundlich isotherm		
	Q_m	K_L	R^2	K_F	n	R^2
Nanospherical MgO	495.05	0.00910	0.978	81.52	3.92	0.986
Plate-like MgO	507.61	0.01187	0.979	31.34	2.17	0.984

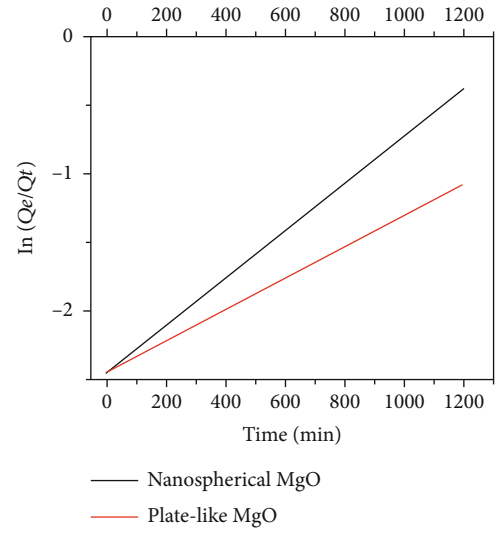

Figure 8: First-order kinetics plots on adsorption of RY on to MgO particles.

The plots drawn between ln (Q_e/Q_t) and t is shown in Figure 8. The rate constant, half-life time ($t1/2$), and linear correlation of RY adsorption of nanospherical MgO are

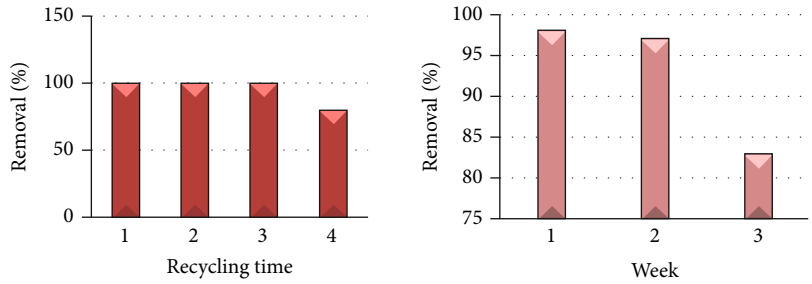

Figure 9: Reusability and durability data for spherical MgO-NPs.

Table 2: Comparison of adsorption capacities of MgO-NPs synthesized by different method for various types of dyes.

Method	Particle size/nm	Dye	Q_m/mg g^{-1}	Reference
Sol-gel	38	Bromophenol blue	40	[39]
		Fast Orange 3R	30	
Green	~10	Congo red	2375	[40]
Hydrothermal	10-20	Methyl orange	370	[41]
		Sudan III	180	
		Congo red	471-588	
Coprecipitation	19	Reactive black 5	500	[42]
		Reactive Orange 122	333.4	
Facile	8.19	Congo red	5000	[43]
Urea assisted	27	Remazol yellow	495	This wok
	23		507	

0.00173 min^{-1}, 400.66 min, and 0.9821, respectively, while the same parameters for the RY adsorption of plate-like MgO are 0.00114 min^{-1}, 608.02 min, and 0.9935, respectively.

3.4. Desorption Study. The UV-vis spectra of desorption for plate-like MgO and nanospherical MgO are given in Figure S4. The desorption amounts of RY dye from the adsorbates of plate-like MgO and nanospherical MgO into distilled water are 13.1 ppm and 14.5 ppm, respectively. That means the percentage desorption of RY from plate-like MgO and nanospherical MgO adsorbates is 1.31% and 1.45%, respectively. The remaining RY could be recovered by digesting the RY-adsorbed MgO particles in a suitable diluted strong acid.

3.5. Evaluation of Adsorption Mechanism. The characterization of data of RY-adsorbed MgO products is very important in understanding the adsorption mechanisms of MgO adsorbates. XRD patterns of RY-adsorbed particles as shown in Figure S5 reveal that MgO has been converted into a brucite crystalline form of Mg(OH)2. The adsorption process of the dye molecule onto the MgO surface goes through a physical attraction which could be both H bonding and electrostatic attraction with the surface. pH of the zero point of charge (pH_{ZPC}) of MgO is 12.1~12.5 [33]. This is favorable for the adsorption of anions onto the positively charged surface due to electrostatic attraction. Reactive dyes are anionic dyes which have negative sulfonate groups. The MgO surface is positively charged during the experimental conditions (pH = 8), and therefore, the Vander walls interaction occurs between the dye molecule and MgO surface. Also, great adsorption occurs through the O-contained functional groups in MgO surface which act as the anchoring sites for RY molecules. There, strong H bonds occur between H atom in the –OH group in the MgO surface and O atom in the S=O group in the RY. Also, H bonding occurs through O atom in the –OH group in the MgO surface and N atoms in the –N=N group in RY [27].

Reactive dyes are hydrophilic dyes. When considering the effect of water composition on the dye adsorption mechanism, mainly, we have to consider the hydration process of the MgO-NP surface, which is the formation of $Mg(OH)_2$. It follows three steps, first, adsorption of water at the surface and simultaneous diffusion of water molecules into inside of porous MgO particles. Then, dissolution of oxide within these particles occurs and leads to changing porosity with time. Finally, supersaturation, nucleation, and growth of $Mg(OH)_2$ on the surface MgO occurs. Formation of $Mg(OH)_2$ layer on the surface of MgO makes an additional resistance which limits the further continuation of the hydration process. Formed $Mg(OH)_2$ also acts as an adsorbent for removal of dye. There are few reports on $Mg(OH)_2$ as an adsorbent [34, 35]. Also, it makes the strong H bond with dye molecules which leads to a strong adsorption. This is a positive impact on adsorption process.

3.6. Durability and Reusability of MgO-NPs. Durability and reusability of MgO-NPs are important parameters in

applications. Both parameters were examined by comparing dye degradation efficiency for both materials. Reusability was examined for a 3-week time duration with one-week time interval. The regenerate data were observed for the first two weeks which are 98% and 97%, respectively. At the end of the 3rd week, the reduction efficiency was 83%. Reusability was examined by continuing 4 recycling times. Regenerated results were obtained for first 3 trials while there was a slight reduction (80%) in adsorption efficiency. This observation (Figure 9) might be due to the aggregation of MgO particles which leads to the reduction in active sites.

MgO-NPs show different properties depending on synthesis methods, i.e., they depend on the calcination temperature and precursor material [36]. The main characteristic parameters of nMgO are morphology, crystal size, crystal structure, density, pore size, total porosity, specific surface area, and reactivity [37, 38]. Many studies have examined dye removal by adsorption on nMgO with different experimental and synthesis conditions with different dyes. So, it is difficult to compare the efficiency of urea-assisted synthesized nMgO on dye removal with other synthesized methods presented by other authors due to the difference in particle size, surface area, morphology, and experimental conditions (Table 2).

MgO shows ferromagnetism (FM) properties when doped with N. N-doped MgO can be prepared by N substituting for O. This can be tried by serial cogrinding of MgO-NPs and urea followed by calcining the product above 400°C [44]. There, one extra hole entirely localizes around the 2p orbitals. This leads to structural defects in MgO rock salt cubic structure which causes in the reduction in the wide band gap of MgO and leads in photoluminescence spectra [45]. This phenomenon is effective for MgO-NPs as a photocatalyst in dye removal process.

4. Conclusions

Spherical-shaped nano-MgO particles and nanoporous plate-like MgO with narrow size distribution have been successfully synthesized using magnesium chloride as the starting material. The final product has been confirmed by XRD, FE-SEM, HR-TEM, FT-IR, and TGA analytical methods. The capability of the product upon adsorbing industrial reactive dye molecules was quantified by BET and UV-vis spectroscopic methods. This method assures low-cost, large-scale production of an efficient dye remover for the urgent need of purification of industrial waste water, as a viable solution

Data Availability

The data can be obtained from the corresponding author, Dr. M.M.M.G.P.G. Mantilaka on request (Email. mantilaka@gmail.com).

Conflicts of Interest

The authors declare that there is no conflict of interest regarding the publication of this paper.

Authors' Contributions

H.M.S.P. Randiligama and M.M.M.G.P.G. Mantilaka contributed to the manuscript equally, and they are considered cofirst authors

Acknowledgments

The authors thank Dr. Nicola Gurusinghe and Dr. R. T. De Silva at Sri Lanka Institute of Nanotechnology for their supports. Sri Lanka Institute of Nanotechnology is acknowledged for funding the research.

Supplementary Materials

Figure S1: 400 ppm RY dye solution (a) before and (b) after adsorption by 0.005 g of nanospherical MgO. Figure S2: fitting the adsorption data of (a) MgO nanospheres and (b) plate-like MgO to the Langmuir isotherm model. Figure S3: Fitting the adsorption data of (a) MgO nanospheres and (b) plate-like MgO to the Freundlich isothermal model. Figure S4: UV-vis spectrum of desorbed RY from (a) plate-like MgO and (b) nanospherical MgO. Figure S5: XRD and SEM of (a) plate-like MgO and (b) spherical MgO nanoparticles after adsorbing RY. Figure S6: FT-IR spectra of (a) bare RY (b) RY-adsorbed spherical MgO nanoparticles and (c) RY-adsorbed plate-like MgO. *(Supplementary Materials)*

References

[1] H. E. Gall and O. Mina, "Coping with emerging contaminants in potable water sources," *Handbook of Environmental Chemistry*, vol. 30, pp. 61–93, 2014.

[2] S. A. Parsons and B. Jefferson, *Organic Removal*, Introduction to Potable Water Treatment Processes- John Wiley and Sons, 2006.

[3] K. E. Lee, N. Morad, T. T. Teng, and B. T. Poh, "Effects of different conditions on the removal of dye from reactive dye wastewater using inorganic-organic composite polymer," *International Journal of Environmental Science and Development*, vol. 3, pp. 1–4, 2012.

[4] N. D. Tissera, R. N. Wijesena, and K. M. N. De Silva, "Ultrasound energy to accelerate dye uptake and dye-fiber interaction of reactive dye on knitted cotton fabric at low temperatures," *Ultrasonics Sonochemistry*, vol. 29, no. 5-6, pp. 270–278, 2016.

[5] K. Pandiselvi, A. Manikumar, and S. Thambidurai, "Synthesis of novel polyaniline/MgO composite for enhanced adsorption of reactive dye," *Journal of Applied Polymer Science*, vol. 131, no. 9, 2014.

[6] M. Kobya, E. Demirbas, and M. Sözbir, "Decolorisation of aqueous reactive dye Remazol Red 3B by electrocoagulation," *Coloration Technology*, vol. 126, no. 5, pp. 282–288, 2010.

[7] G. Muthuraman and K. Palanivelu, "Removal of CI reactive yellow 125, CI reactive red 158 and CI reactive red 159 dyes from aqueous solution with a supported liquid membrane containing tributylphosphate as carrier," *Journal of the Textile Institute*, vol. 97, no. 4, pp. 341–348, 2006.

[8] L. Q. Chai, J. Z. Shao, and L. Zhou, "Dyeing kinetics of gardenia yellow on cotton," *Journal of Textile Research*, vol. 31, pp. 212–216, 2010.

[9] T. N. Borisova, K. N. Demidov, O. F. Shatilov et al., "Improving lining resistance using high-magnesia fluxes in the converter steelmaking process," *Refractories and Industrial Ceramics*, vol. 44, pp. 13–16, 2003.

[10] A. V. Zabolotskii, "Mathematical simulation of the thermal stability of magnesium oxide," *Refractories and Industrial Ceramics*, vol. 52, no. 3, pp. 170–177, 2011.

[11] B. Elgquist and M. Wedborg, "Stability constants of $NaSO_4^-$, $MgSO_4$, MgF^+, $MgCl^+$ ion pairs at the ionic strength of seawater by potentiometry," *Marine Chemistry*, vol. 6, no. 3, pp. 243–252, 1978.

[12] K. Ravichandran, S. Vaishnavi, and D. Nedumaran, "Synthesis and characterization of nanocrystalline MgO for optical applications using sol-gel method," *Advanced Materials Research*, vol. 646, pp. 76–83, 2013.

[13] G. Dercz, L. Pająk, K. Prusik, R. Pielaszek, J. J. Malinowski, and W. Pudło, "Structure analysis of nanocrystalline MgO aerogel prepared by sol-gel method," *Solid State Phenomena*, vol. 130, pp. 203–206, 2007.

[14] M. Zieliński, A. Kiderys, M. Pietrowski, B. Czajka, I. Tomska-Foralewska, and M. Wojciechowska, "MgO modified with MgF2 as an electrolyte immobilizing agent for the high-temperature cells," *Applied Sciences*, vol. 9, no. 13, p. 2642, 2019.

[15] X. Tang, Y. Nie, Q. Jin et al., "Kinetics and mechanism of ultrasonic- assisted magnesium oxide hydration," *Ultrasonics Sonochemistry*, vol. 40, Part A, pp. 995–1002, 2018.

[16] N. Takahashi, "Simple and rapid synthesis of MgO with nanocube shape by means of a domestic microwave oven," *Solid State Sciences*, vol. 9, no. 8, pp. 722–724, 2007.

[17] Y. C. Hong and H. S. Uhm, "Synthesis of MgO nanopowder in atmospheric microwave plasma torch," *Chemical Physics Letters*, vol. 422, no. 1-3, pp. 174–178, 2006.

[18] J. Jeevanandam, Y. S. Chan, and M. K. Danquah, "Biosynthesis and characterization of MgO nanoparticles from plant extracts via induced molecular nucleation," *New Journal of Chemistry*, vol. 41, no. 7, pp. 2800–2814, 2017.

[19] V. S. Vendamani, A. Tripathi, A. P. Pathak, S. V. Rao, and A. Tiwari, "Laser ablation of natural micas: synthesis of MgO and Mg(OH)2 nanoparticles and nanochains," *Materials Letters*, vol. 192, pp. 29–32, 2017.

[20] Y. Yin, G. Zhang, and Y. Xia, "Synthesis and characterization of MgO nanowires through a vapor-phase precursor method," *Advanced Functional Materials*, vol. 12, no. 4, pp. 293–298, 2002.

[21] G. Sharma and P. Jeevanandam, "Synthesis of transition metal oxide based MgO nanocomposites by a simple precursor approach," *Advanced Materials Research*, vol. 585, pp. 169–173, 2012.

[22] C. K. Muoto, E. H. Jordan, M. Gell, and M. Aindow, "Effects of precursor chemistry on the structural characteristics of Y_2O_3-MgO nanocomposites synthesized by a combined sol-gel/thermal decomposition route," *Journal of the American Ceramic Society*, vol. 94, no. 2, pp. 372–381, 2011.

[23] C. Quintanar, R. Caballero, and V. M. Castaño, "Adsorption of CO on the rumpled MgO(100), MgO(100):Ni, and MgO(100):Cr surfaces: a density functional approach," *International Journal of Quantum Chemistry*, vol. 102, no. 5, pp. 820–828, 2005.

[24] T. Sawada, K. Watanabe, K. Fukuyama, T. Ohira, M. Kinugawa, and K. Sano, "The Gas adsorption characteristics of MgO films for PDP deposited under oxygen atmosphere," *Shinku*, vol. 43, no. 10, pp. 973–977, 2000.

[25] S. Jalili, R. Majidi, and K. Ghafoori Tabrizi, "The effect of gas adsorption on the electronic properties OFMgOANDCa-DOPEDMgO," *Journal of Theoretical and Computational Chemistry*, vol. 6, no. 4, pp. 803–810, 2007.

[26] A. N. M. Salem, M. A. Ahmed, and M. F. El-Shahat, "Selective adsorption of amaranth dye on Fe3O4/MgO nanoparticles," *Journal of Molecular Liquids*, vol. 219, pp. 780–788, 2016.

[27] R. M. Mohamed, A. Shawky, and I. A. Mkhalid, "Facile synthesis of MgO and Ni-MgO nanostructures with enhanced adsorption of methyl blue dye," *Journal of Physics and Chemistry of Solids*, vol. 101, pp. 50–57, 2017.

[28] G. Moussavi and M. Mahmoudi, "Removal of azo and anthraquinone reactive dyes from industrial wastewaters using MgO nanoparticles," *Journal of Hazardous Materials*, vol. 168, no. 2-3, pp. 806–812, 2009.

[29] A. K. Sharma and B. K. Lee, "Surfactant-aided sol-gel synthesis of TiO_2 –MgO nanocomposite and their photocatalytic azo dye degradation activity," *Journal of Composite Materials*, vol. 54, no. 12, pp. 1561–1570, 2020.

[30] S. Mahdavi, M. Jalali, and A. Afkhami, "Heavy metals removal from aqueous solutions using TiO_2, MgO, and Al2O3NANOPARTICLES," *Chemical Engineering Communications*, vol. 200, no. 3, pp. 448–470, 2013.

[31] K. Mageshwari, S. S. Mali, R. Sathyamoorthy, and P. S. Patil, "Template-free synthesis of MgO nanoparticles for effective photocatalytic applications," *Powder Technology*, vol. 249, pp. 456–462, 2013.

[32] S. Jorfi, G. Barzegar, M. Ahmadi et al., "Enhanced coagulation-photocatalytic treatment of acid red 73 dye and real textile wastewater using UVA/synthesized MgO nanoparticles," *Journal of Environmental Management*, vol. 177, pp. 111–118, 2016.

[33] J. C. Crittenden, R. R. Trussell, D. W. Hand, K. J. Howe, and G. Tchobanoglous, *MWH's Water Treatment: Principles and Design: Third Edition*, John Wiley and Sons, Inc, 2012.

[34] T. N. Ramesh and V. Pavagada Sreenivasa, "Removal of indigo carmine dye from aqueous solution using magnesium hydroxide as an adsorbent," *Journal of Materials*, vol. 2015, Article ID 753057, 10 pages, 2015.

[35] X. N. Zhang, G. Y. Mao, Y. B. Jiao, Y. Shang, and R. P. Han, "Adsorption of anionic dye on magnesium hydroxide-coated pyrolytic bio-char and reuse by microwave irradiation," *International Journal of Environmental Science and Technology*, vol. 11, no. 5, pp. 1439–1448, 2014.

[36] A. Kumar and J. Kumar, "On the synthesis and optical absorption studies of nano-size magnesium oxide powder," *Journal of Physics and Chemistry of Solids*, vol. 69, no. 11, pp. 2764–2772, 2008.

[37] F. Jin and A. Al-Tabbaa, "Characterisation of different commercial reactive magnesia," *Advances in Cement Research*, vol. 26, no. 2, pp. 101–113, 2014.

[38] J. N. Sahu, H. Zabed, R. R. Karri, S. Shams, and X. Qi, "Applications of nano-biotechnology for sustainable water purification," in *Industrial Applications of Nanomaterials*, pp. 313–340, 2019.

[39] M. A. Ahmed and Z. M. Abou-Gamra, "Mesoporous MgO nanoparticles as a potential sorbent for removal of fast orange and bromophenol blue dyes," *Nanotechnology for Environmental Engineering*, vol. 1, no. 1, 2016.

[40] H. Zhang, J. Hu, J. Xie, S. Wang, and Y. Cao, "A solid-state chemical method for synthesizing MgO nanoparticles with superior adsorption properties," *RSC Advances*, vol. 9, no. 4, pp. 2011–2017, 2019.

[41] X. Li, W. Xiao, G. He, W. Zheng, N. Yu, and M. Tan, "Pore size and surface area control of MgO nanostructures using a surfactant-templated hydrothermal process: high adsorption capability to azo dyes," *Colloids and Surfaces A: Physicochemical and Engineering Aspects*, vol. 408, pp. 79–86, 2012.

[42] N. Jamil, M. Mehmood, A. Lateef, R. Nazir, and N. Ahsan, "MgO nanoparticles for the removal of reactive dyes from wastewater," *Advanced Materials - TechConnect Briefs*, vol. 1, pp. 353–356, 2015.

[43] M. Zare, "Facile synthesis of hollow mesoporous MgO nanospheres as ultra-high performance and reusable adsorbent," *Journal of Dispersion Science and Technology*, pp. 1–8, 2020.

[44] J. Lu, Q. Zhang, J. Wang, F. Saito, and M. Uchida, "Synthesis of N-doped ZnO by grinding and subsequent heating ZnO-urea mixture," *Powder Technology*, vol. 162, no. 1, pp. 33–37, 2006.

[45] N. Pathak, P. S. Ghosh, S. K. Gupta, R. M. Kadam, and A. Arya, "Defects induced changes in the electronic structures of MgO and their correlation with the optical properties: a special case of electron–hole recombination from the conduction band," *RSC Advances*, vol. 6, no. 98, pp. 96398–96415, 2016.